Hindawi
Shock and Vibration
Volume 2022, Article ID 3144545, 10 pages
https://doi.org/10.1155/2022/3144545

Research Article

Calculation Model of the Axial Dispersion Distribution of Cylindrical-Warhead Fragments

Ning Jiang, Wen Bin Li, Wen Jin Yao, and Da Cheng Gao

ZNDY Ministerial Key Laboratory, Nanjing University of Science and Technology, Nanjing 210094, China

Correspondence should be addressed to Wen Bin Li; lwb2000cn@njust.edu.cn

Received 20 October 2021; Accepted 29 December 2021; Published 31 January 2022

Academic Editor: Letícia Fleck Fadel Miguel

The dispersion distribution characteristics of prefabricated fragments from an improvised explosive device (IED) are essential in defense technology development. To improve warhead design, it is essential to predict a fragment's velocity and dispersion distribution accurately. This paper investigates a fragment's flying angle from a detonated warhead with a cylindrical charge under a one-end central detonation. A modified formula for calculating the fragment dispersion distribution at each axial position of the warhead was obtained based on experimental data and model analysis. The impacts of the following parameters on the flying angle were considered in the formula: ratio of charge mass to shell mass, charge diameter, axial sparse effect, and relative axial shell position. The formula was verified by experimentation to be suitable for wide applications using different validation samples. Theoretical calculations with the formula show good accuracy in predicting the flying angle of cylindrical-shell fragments, agreeing with experimental data. The proposed model meets the error requirements of engineering applications. This work provides a theoretical foundation for subsequent research on damage effectiveness and IED damage assessment.

1. Introduction

A cylindrical charge warhead filled with fragments (e.g., metal balls) is a typical structure for warhead design and is called a fragmentation warhead [1]. After detonation, the high-pressure fragments are transported at high velocities and are the primary source of damage [2]. Being able to predict the fragment's trajectory accurately will improve warhead design. Previous researchers have proposed a series of empirical formulas to estimate the performance of cylindrical charge warheads. Among these formulas, the Gurney formula is representative in calculating the fragment's velocity as follows [3]:

$$V_{\text{Gurney}} = \sqrt{2E}\sqrt{0.5 + 1/\beta}, \tag{1}$$

where V_{Gurney} is the initial velocity of the fragment, $\sqrt{2E}$ is the Gurney energy, and β is the ratio of charge mass to shell mass. The Gurney formula does not consider the sparse wave effect on the fragment's velocity at the two ends of the warhead [4]. After the Gurney formula was proposed, many researchers have improved his theory. For example, Zulkoski [5] and Randers Pehrson [6] independently proposed their methods to modify the Gurney formula. However, their model yields large errors for the terminal velocity. Therefore, Huang et al. [4] proposed a more accurate formula to try to estimate the fragment's velocity of a cylindrical shell detonated at one end as follows:

$$V_{\text{Huang}} = \left(1 - 0.361\,\mathrm{e}^{-1.111x/d}\right) \cdot \left(1 - 0.192\,\mathrm{e}^{-3.03\,(L-x)/d}\right)\sqrt{2E}\sqrt{0.5 + 1/\beta}, \tag{2}$$

where L and d are the length and inner diameter of the cylindrical shell, respectively, and x is the axial distance from the detonation location ($0 \le x \le L$, where $x = 0$ represents the detonation location). This formula has been widely used and is a modification to the Gurney formula by applying the axial sparse wave effect.

To predict the warhead flying angle, Taylor [7] proposed a representative analytical formula as follows:

$$\sin\left(\frac{\theta}{2}\right) = \frac{V_0}{2\,D}, \tag{3}$$

where D is the detonation velocity of the explosive, and $\theta/2$ is the angle between the fragment's flying direction and the normal direction of the projectile body, which is called the "Taylor angle." Figure 1 is adapted from Felix et al. [8], Carlucci and Jacobson [9], Deshpande [10], and Walters and Zukas [11], representing the variables in the Taylor formula. Here, V_N is the fragment's velocity when the fragment's flying direction is 90° from the fragment, and V_A is the fragment's velocity when the fragment's flying direction is 90° from the shell's axial direction. Many experimental data have shown that the Taylor formula is inaccurate in predicting a fragment's flying angle, especially for the fragments near the two ends of the warhead.

To improve the accuracy of the Taylor formula, many researchers [12–17] have modified the calculation approach of the Taylor angle. However, there are still significant calculation errors found when compared with empirical data. Other researchers [18, 19] proposed an equation based on a simplified simulation method to estimate the initial flying angle of the fragment by applying the influence of fragment acceleration as follows:

$$\delta = \frac{V_0}{2\,D}\sin\alpha_e - \frac{1}{2}\tau_e V\prime, \tag{4}$$

where τ_e is a characteristic acceleration time, and V' is the spatial derivative of the fragment's initial velocity along the axial direction of the warhead. It is not easy to estimate these two parameters. Moreover, they cannot be measured experimentally so can only be obtained by simulation. Therefore, this formula has considerable limitations.

Felix et al. [8] proposed formulas to calculate the initial flying angle based on shell expansion shape as follows:

$$\delta = \left(\frac{180}{\pi}\right)\left(\frac{1}{\lambda}\right)\tan^{-1}\left(-0.33 \times 4\left(\frac{(x-M)^3}{(M)^4}\right)\right) + \theta\,(0 \le x \le M). \tag{5}$$

$$\delta = \left(\frac{180}{\pi}\right)\left(\frac{1}{\lambda}\right)\tan^{-1}\left(-0.33 \times 4\left(\frac{(x-M)^3}{(1-M)^4}\right)\right) + \theta\;(M \le x \le 1), \tag{6}$$

where λ is the expansion coefficient of the shell measured from the detonation end (denote $\lambda = 1$ at 20% of the axial distance away from the detonation end), and x is the axial position relative from the detonation end; $M = 0.6$ assumes that both the shell expansion and the fragment's flying velocity reach their maximum values at the relative axial position of 0.6. The use of this formula (6) requires known inputs of the fragment's flying angle reduction at the end-plate and the position of the maximum fragment velocity. It is difficult to obtain these two input data experimentally. Therefore, the relative position and reduction accuracy are mostly assumed values and hence inaccurate. Thus, the above-modified formulas also have significant limitations.

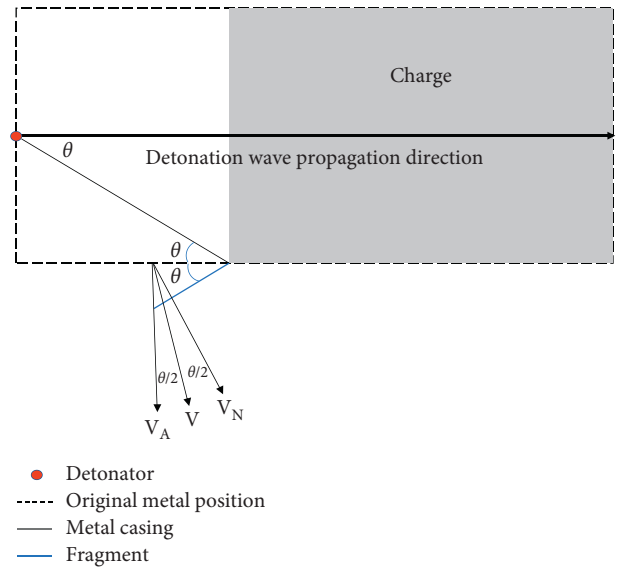

Figure 1: Variables used in Taylor equation.

In order to overcome the disadvantages in the models mentioned above, in terms of the impact of the axial sparse effect on the fragment dispersion distribution, this paper proposes a model to predict the dispersion distribution of the cylindrical warhead under one-end detonation by considering the axial sparse effect and the relative position along the shell's axial direction. The model was developed based on the experimental data using different ratios of charge mass to shell mass and different charge diameters. Experimental data of a fragment's initial velocity and flying angle under different sample conditions were obtained. The impacts of the detonation wave reaction and sparse wave propagation on fragment dispersion were analyzed. Parametric function curves derived from the proposed model were established. Finally, the theoretical model was validated by using static detonation tests.

2. Samples and Experimental Layout

In order to study the axial dispersion characteristics of the fragments driven by an explosion, a static explosion test was carried out on an explosive device, as shown in Figure 2. The spatial fragment distribution was measured by the penetration positions on a witness plate. The sample explosive was placed on flat plank support 1.5 m above the ground. The witness plate was made of carbon structural steel and had dimensions of 1570 mm in length, 3000 mm in height, and 3 mm in thickness. The covering angle between the warhead and the witness plate was 18°. The witness plate was placed 5 m away from the warhead. The detonation method was a one-end detonation from the center. The test sample was placed vertically with the detonation end facing upward. A high-speed camera system, which included a FASTCAM ultima APX high-speed camera produced by the Photron Company, was used to monitor and record the fragment's perforation process through the target witness plate. The camera shooting rate was set at 13,000 frames per second.

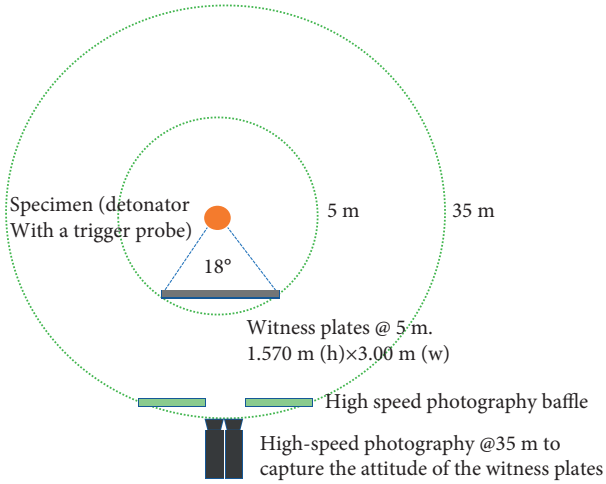

Figure 2: Schematic view of experimental setup (top view).

The horizontal distance between the explosion-driven device of the warhead and the high-speed camera was 35 m. After the test, the witness plate was recycled and photographed to obtain perforation conditions, and the perforation positions were measured.

According to the structure shown in Figure 3, six sets of cylindrical specimens with different internal diameters and aspect ratios (i.e., the ratio of length to diameter) were prepared. The cylindrical samples were equipped with the JH-2 explosive, 45 steel sleeves with a 3 mm thickness, side end covers with a 5 mm thickness, and steel balls with a 5 mm diameter. The charge was pressed into the samples under a 300 MPa pressure using 300-ton pressing equipment to obtain a charge density greater than 1.69 g/cm^3. The internal and external sleeves were fixed using a threaded connection. The 5 mm diameter steel ball fragments were put into the sleeve in sequence. An epoxy resin was injected into the sleeve to fix the steel balls. All samples had the same density of the 8,701 explosives and the same sleeve thickness. The length-to-diameter ratios of the six samples were 2 : 1, 1.8 : 1, and 1.6 : 1, and the charge diameters were 56 mm, 70 mm, and 89 mm. The charge mass to shell mass ratios (C/M) of the six samples were 0.778, 0.579, and 0.743. Table 1 lists detailed specifications of the samples.

3. Experimental Results

3.1. Analysis of High-Speed Photography Results. The high-speed camera recorded the fragment's perforation process through the target witness plate. According to the time marks on the photo, the fragment's velocity at a given distance was calculated to obtain all the fragment data within the coverage angle of the witness plate. After the test, the image was converted into the grayscale bitmap, and brightness and contrast were adjusted using a data acquisition system connected to the high-speed camera to reveal the process of fragment perforation, as shown in Figure 4.

Figure 4 shows that obvious firelight appeared on both sides of the witness plate after the charge exploded. As time went by, the firelight's brightness first increased and then

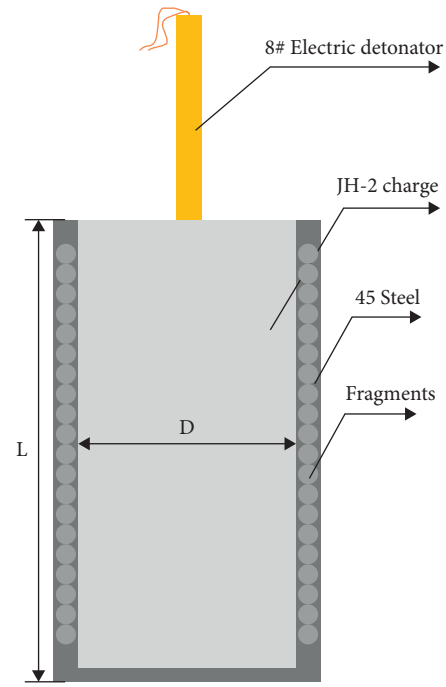

Figure 3: Schematic diagram of the sample structure.

gradually decreased. The frame before the firelight occurrence was set to 0 in the time scale. It was found that after the charge explosion, the firelight produced by fragment perforation on the witness plate appeared at 30.8 ms and lasted till 38.4 ms. The fragments spread and increased from the center of the witness plate to both sides. The increased number of fragments on the lower part of the witness plate was greater than that on the upper part. The fragment's flying velocity first increased and then decreased from the detonation end to the explosion center and then to the other end. In order to calculate the fragment's trajectory, the trajectory of the fragment was assumed horizontal, and the impacts of air lift and gravity were ignored. Thus, only the effect of air resistance was considered. According to the velocity attenuation formula of a spherical fragment, the fragment's motion equation was expressed as follows:

$$m_{\mathrm{f}}\frac{\mathrm{d}v}{\mathrm{d}t} = -\frac{1}{2}c_{\mathrm{f}}\rho_0\overline{A}v^2, \tag{7}$$

where v is the instantaneous velocity of the fragment, c_f is the air resistance coefficient of fragment flying ($c_f = 0.97$ for a spherical prefabricated fragment), and $\overline{A}$ is the average windward area of the fragment. Equation (7) was integrated to obtain the following equation that links the fragment flying velocity v_f and the flying time t_f:

$$v_f = \frac{v_0}{1 + c_f\rho_0\overline{A}v_0t_f/\left(2m_f\right)}. \tag{8}$$

According to the above equation, the fragment's initial velocity was calculated based on the measured velocity. Then, these data were used as a basis for establishing a model to predict the dispersion distribution of the cylindrical warhead under one-end detonation. The measured values of

Table 1: Parameter specifications of cylindrical-warhead samples with charge and fragments.

Sample	Charge parameter				Warhead shell parameter					Ratio of charge mass to shell mass, C/M
	Diameter, D (mm)	Length, L (mm)	Mass, m (g)	Density, ρ (cm^3)	Shell thickness, D_c (mm)	Shell mass, m (g)	Fragment diameter, D_p (mm)	Fragment mass, m (g)	Density, ρ (cm^3)	
1	56	112	467.6	1.695	3	202.4	5	398.6	7.83	0.778
2	56	112	467.6	1.695	3	202.4	5	398.7	7.83	0.778
3	70	126	821.4	1.694	3	561.8	5	856.8	7.83	0.579
4	70	126	821	1.693	3	561.8	5	856.8	7.83	0.579
5	89	142.4	1502.5	1.696	3	1201.9	5	820.3	7.83	0.743
6	89	142.4	1501.6	1.695	3	1201.3	5	820.3	7.83	0.743

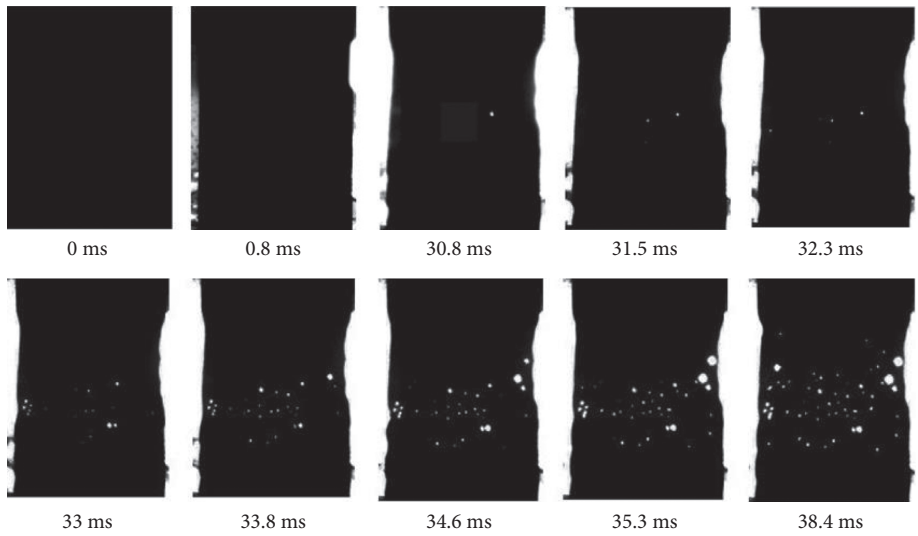

Figure 4: Target penetration process of prefabricated fragments driven by explosion.

initial warhead velocity by using the high-speed camera are shown in Table 2.

3.2. Witness Plate Analysis. After the test, fragment perforation on the witness plate was analyzed. The sudden change in the gray value of each edge pixel of the perforated hole was used to segment the image, identify the target hole area, and extract the hole shape. The Image-Pro Plus (IPP) and Image J analysis software packages were used to measure and locate the contour of the hole on the witness plate. The number of holes was counted, as shown in Figure 5.

Because the perforated hole was the same as the fragment in both size and shape, the IPP technique was effectively used to obtain the perforated holes produced by the prefabricated fragments. The perforation conditions of the six warhead samples were collected and analyzed to obtain their fragment dispersion distributions. The samples with the same ratio of length to diameter had consistent dispersion distributions. The test data were reliable with few experimental errors, and therefore, they were used to build a model to predict the fragment dispersion distribution, as shown in Figure 6.

The derived fragment dispersion distribution curves showed that the warheads with different aspect ratios were affected by the sparse waves at the two ends of the shell,

Table 2: Measured values of the initial velocity of the warhead fragment.

Sample	Diameter, D (mm)	Length, L (mm)	Warhead fragment initial velocity, V_0 (m/s)
1	56	112	1764
2	56	112	1753
3	70	126	1593
4	70	126	1570
5	89	142.4	1748
6	89	142.4	1756

exhibiting similar nonlinear distributions. The fragments in the middle part flew steadily, and the fragments at the two ends flew with more deviated flying angles. The decrease or increase in the flying angles at the two ends depended on the end effect of the sparse waves, which mainly affected the dispersion distributions on the detonating and nondetonating ends; the detonation end was more affected by the sparse wave than the nondetonation end. As mentioned above, when the explosion was detonated, the axial sparse wave was rapidly transmitted from the detonation end to the explosion products, inhibiting the load given by the detonation wave near the detonation end. The axial sparse wave propagating from the nondetonation end to the explosion products was generated only when the detonation wave

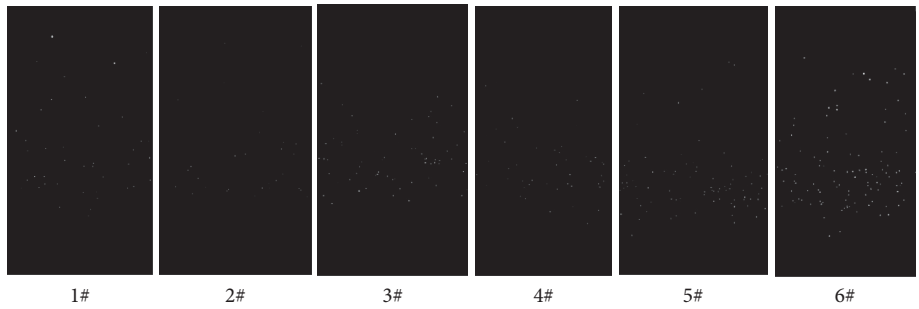

Figure 5: Picture of pit treatment on witness plate after test.

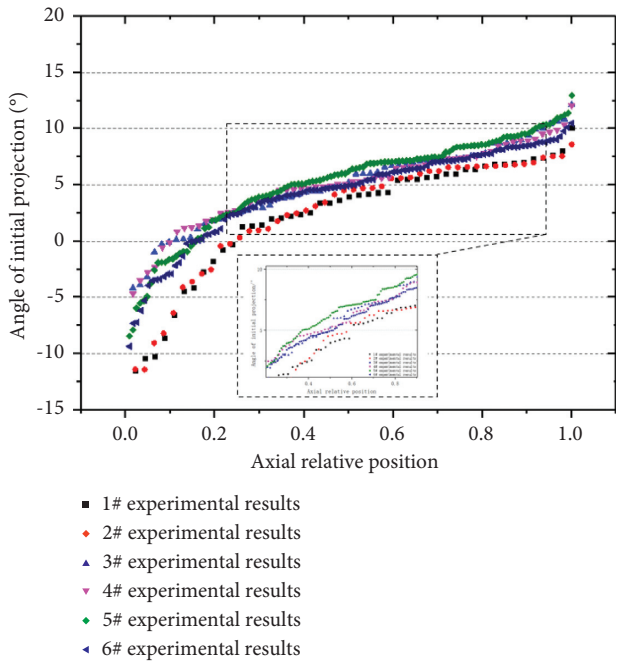

Figure 6: Test value of combat fragmentation dispersion distribution.

propagated to the nondetonation end. Therefore, the nondetonation end was only affected by the axial sparse wave in a very small time interval, and the corresponding fragment flying angle was less affected. The flying angle presented a distribution trend that it first rapidly increased in an arc pattern, then became flat, and finally slowly increased in an exponential form. The impacts of the axial sparse waves at the two ends on the fragment's flying angle gradually separated. The explosion-driven dispersion in the middle part of the shell gradually completed in an intermediate transition period of the axial sparse wave. Therefore, the effects of the axial sparse waves from the two ends on fragments flying off the middle part were gradually weakened.

4. Model Establishment

4.1. Empirical Model Establishment of the Flying Angle. It is necessary to establish an empirical model to describe the fragment dispersion to study further the impact of the axial sparse waves under different charge diameters and aspect ratios on the dispersion distribution. Based on the above test results of dispersion distribution, the fragment dispersion distribution curve was similar to a hyperbolic sine curve (sinhx) in their function variation characteristics. The hyperbolic sine curve was translated and processed by coefficient transformation so that the curve had positive and negative values at $x = 0 - 1$ (relative position in the axial direction). Therefore, such a new hyperbolic sine function was obtained as follows:

$$f(x) = \sinh x = \frac{e^{x} - e^{-x}}{2} = \sum_{n=0}^{\infty} \frac{x^{2n+1}}{(2n+1)!}. \tag{9}$$

This function is an odd function that can be decomposed into a convex function and a concave function that is monotonically increasing. The hyperbolic cosine curve could not construct the empirical model because there were negative values in the fragment dispersion curves obtained experimentally.

Previous formulas could not reflect the actual trajectories of warhead fragments under the impact of the sparse waves at the two ends of the shell. The detonation wave had different shapes at different axial positions, causing different impulses and pressures sustained by the inner wall of the shell and different loads along the axial direction at different positions along the projectile body. Therefore, there was an axial expansion in the projectile. Related terms of the sparse waves at the two ends were introduced to the model to describe the propagation of the axial sparse waves towards the two free ends to correct the predicted fragment flying angle.

As shown in Figures 7 and 8, the dispersion distribution was affected by the coupling effect of the axial sparse waves from the two ends. Huang et al. [4] studied the fragment velocity distribution of a warhead with a charge of a large aspect ratio. They found that the empirical formula of a single variable could not describe the interaction between them. They proposed a widely used two-variable three-dimensional empirical formula to determine the coupling effect of the sparse waves on the fragment dispersion distribution at different coaxial positions. This paper proposes a modification by using a fragment dispersion distribution model $\tan\theta(x, y)$ to cover the effect of different aspect ratios as follows:

$$\theta(x, y) = f(x) \cdot f(y) \cdot \theta, \tag{10}$$

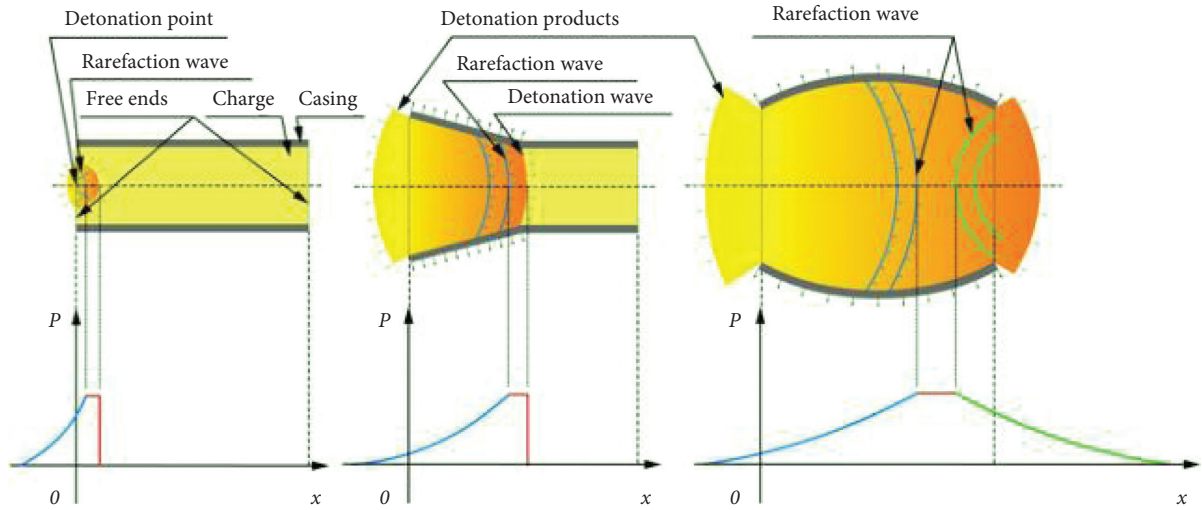

Figure 7: Sparse wave propagation diagram at two free ends of the sleeve.

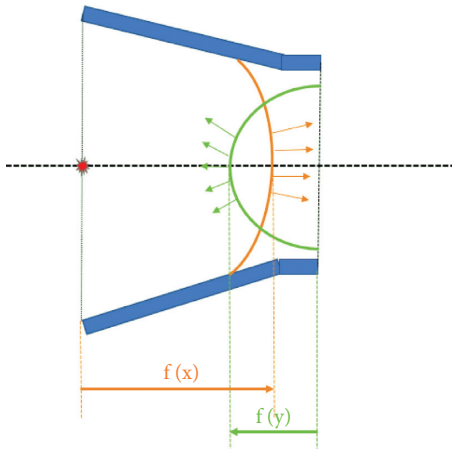

Figure 8: Schematic diagram of axial sparse waves at the detonation and nondetonation ends.

where the independent variable $x = Lx/D$ is the proportional distance of the fragment to the detonation end, $y = Ly/D$ is the proportional distance of the fragment to the nondetonation end, θ is an ideal fragment dispersion distribution model without the impact of the axial sparse waves. $f(x)$ and $f(y)$ represent the impacts of the axial sparse waves from the detonation and nondetonation ends on the fragment dispersion distribution, respectively.

The Taylor formula can explain the impact of the axial sparse waves on the dispersion distribution at the two ends. It can also explain why the impact of the axial sparse waves on the maximum flying angle changes with an increase in L/D as a hyperbolic sine function. Based on the empirical model of fragment dispersion using the hyperbolic sine function, the modified term for the detonation end can be constructed as follows:

$$f(x) = (a_1 + \sinh(b_1 \cdot x/d)), \tag{11}$$

where a_1 and b_1 are the correction coefficients reflecting the impact of the sparse waves from the detonation end. Similarly, the correction formula for the nondetonation end can be expressed as

$$f(y) = (a_2 + \sinh(b_2 \cdot (L - x)/d)), \tag{12}$$

where a_2 and b_2 are the correction coefficients reflecting the impact of the sparse waves from the nondetonation end.

Therefore, the calculation model of fragment dispersion distribution can be further developed as follows by using the empirical model with the hyperbolic sine function and the Taylor formula:

$$\theta(x, y) = (a_1 + \sinh(b_1 \cdot x/d)) \cdot (a_2 + \sinh(b_2 \cdot (L - x)/d)) \cdot \frac{180}{\pi} \cdot \tan^{-1}\left(\frac{V_0}{2D}\cos\Phi\right). \tag{13}$$

Test data were substituted into the above model, and the data were fitted with a nonlinear least square regression equation. The modified distribution function curve of the flying angle is shown in Figure 9. Test data determined the correction coefficients. The fitted correction result is as follows:

$$\theta(x, y) = \left(-0.138 + \sinh\left(\frac{x}{d}0.409\right)\right) \cdot (4.415 + \sinh(1.47(L - x)/d)) \cdot \frac{180}{\pi}\tan^{-1}\left(\frac{V_0}{2D}\cos\Phi\right). \tag{14}$$

4.2. Model Error Analysis. The R^2 value of parameter fitting was 0.9885, indicating that equation (14) fit the test data very well and describe the fragment dispersion distributions under the impact of the sparse waves for different diameters and charge aspect ratios, especially the dispersion distributions at the detonation and nondetonation ends. The proposed model significantly improves prediction accuracy on warhead damage capability. Due to the inclusion of the parameters of x/d and $(L - x)/d$, the proposed model can

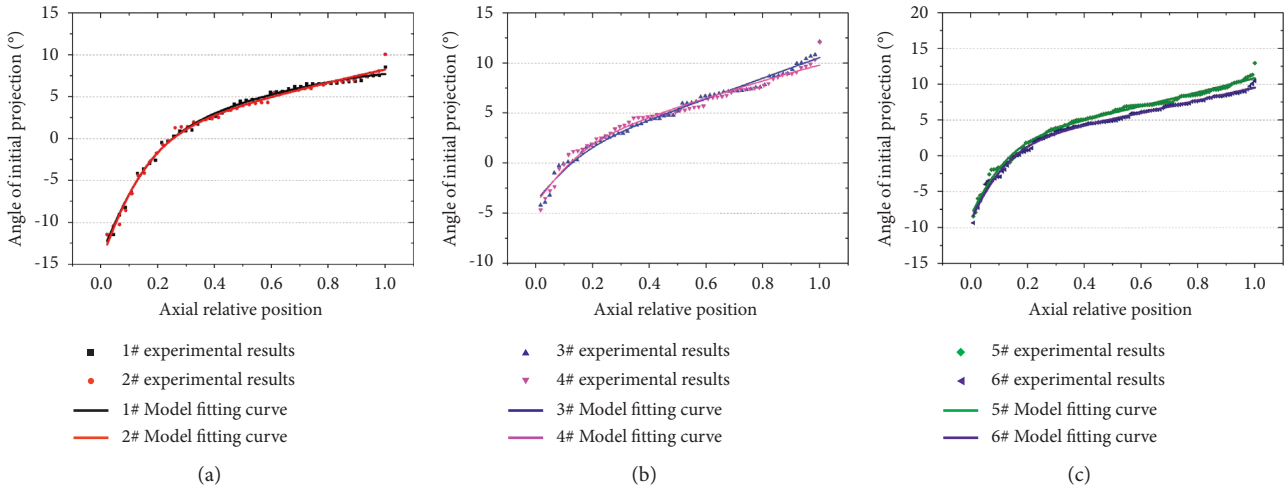

Figure 9: Model fitting curve. (a) 56 mm caliber model fitting. (b) 70 mm caliber model fitting. (c) 89 mm caliber model fitting.

accurately predict the fragment dispersion distribution at each axial position of the cylindrical warhead under one-end detonation. Therefore, the model has significant improvement in accuracy and application range.

Figure 10 shows the comparison between the calculation result and test data. The degrees of freedom (DF), sum of squares, and mean square values of the residuals are 72, 12.86, and 0.19938, respectively. The residuals between the relative axial position and the fitted Y value are mainly distributed between −1 and 1.5, as shown in Figures 10(a) and 10(b). With the line passing the points (−0.93, 0.66) and (0.93, 99.33) as a reference line, the conventional residuals of the percentile are no more than 0.3, as shown in Figure 10(c). The model-fitting results are accurate and in good agreement with the test data. The relative errors of 97% of the data at all axial positions are within 3%. The average error of the six warhead samples is within ±2%. Some large relative errors are due to the impact of the sparse waves from the detonation and nondetonation ends, causing uneven forces acting on the fragments, and hence, dispersion distributions are unstable. The proposed model can largely avoid these errors. In general, this empirical model can be used to calculate the fragment dispersion distribution under the effect of the sparse waves with one-end detonation for a cylindrical charge warhead.

5. Test Verification to Validate the Model

5.1. Samples. In order to verify the universal applicability of the proposed model, several different cylindrical charge warheads were designed. Two samples with the JH-2 explosive were assembled with an aluminum shell, a charge diameter of 30 mm, and a length-to-diameter ratio of 2 : 1. The C/M ratio of the specimen was 0.295. The sleeve thickness was 2 mm. The prefabricated fragment was a tungsten ball of 3 mm diameter. Other detailed structural parameters are listed in Table 3. The JH-2 explosive used in the validation warhead samples was taken from the same batch of the explosive used in earlier tests. The charge was pressed at a 300 MPa pressure with 300 -ton pressing equipment to obtain a charge density greater than 1.69 g/cm^3. The charge length of each specimen was the same as the sleeve length. The test site layout is also shown in Figure 2.

5.2. Model Verification Results. According to the high-speed camera photography results and the fragment velocity attenuation formula, the fragment's initial velocity was calculated based on the measured velocity at the measurement location. The initial fragment velocities of the two test samples were 1205 m/s and 1213 m/s.

The fragment dispersion and target penetration conditions were analyzed by using the witness plate after the test. The images were processed with the previously mentioned approach using the IPP image analysis software to measure the contours of the perforated holes and determine their positions on the witness plate, as shown in Figure 11. The fragment dispersion distribution was obtained by effectively extracting the perforation information from the witness plate, and the proposed empirical formula was used to calculate the fitted dispersion curves. The comparison between the validation test data and the model prediction is shown in Figure 12.

5.3. Model Verification Error Analysis. The R^2 value of parameter fitting was 0.934, indicating a good fit between the model and the validation test data. Figure 13 shows the relative difference between the model result and test data. The DF, sum of squares, and mean square values of the residuals are 56, 56.48, and 1.22, respectively. The residuals between the relative axial position and the fitted Y value are mainly distributed between −2 and 0, as shown in Figures 13(a) and 13(b). With the line passing the points (−2.49, 0.62) and (0.82, 99.37) as a reference line, the conventional residuals of the percentile are no more than 0.4, as shown in Figure 13(c). The model-fitting results are accurate and in good agreement with the validation test data. The relative errors of 97% of the data at all axial positions are within 6%. The average error of the two warhead samples is within ±7%.

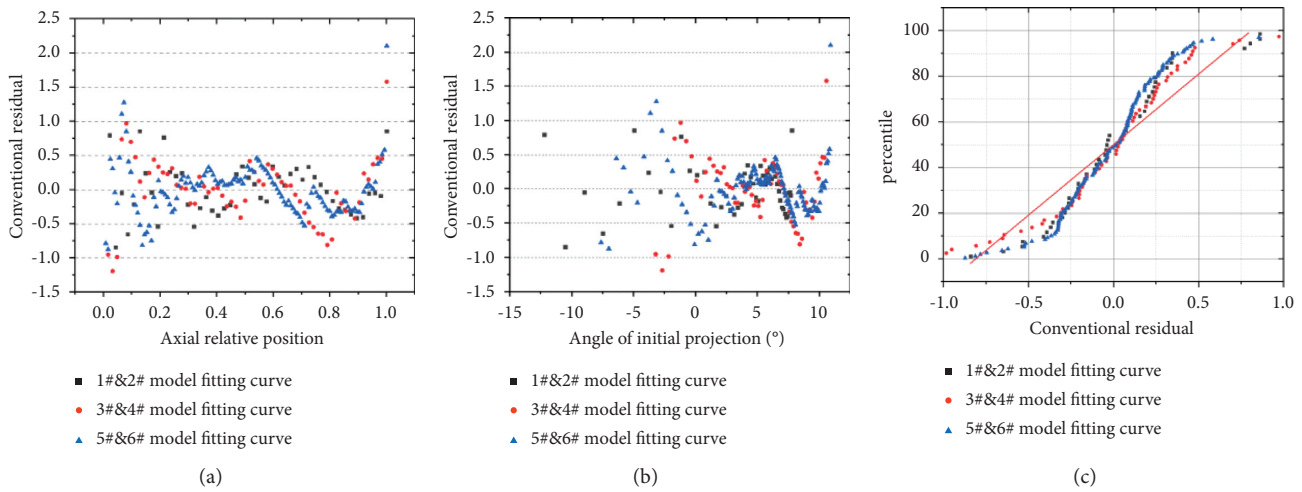

Figure 10: Error analysis of fragmentation dispersion model. (a) Axial relative position error. (b) Dispersion distribution error. (c) Percentile error.

Table 3: Specimen parameters used in the validation test for the proposed model.

Sample	Charge parameter				Warhead shell parameter					Ratio of charge mass to shell mass, C/M
	Diameter, D (mm)	Length, L (mm)	Mass, m (g)	Density, ρ (cm^3)	Shell thickness, D_c (mm)	Shell mass, m (g)	Fragment diameter, D_p (mm)	Fragment mass, m (g)	Density, ρ (cm^3)	
S-1	30	60	71.9	1.695	2	40	3	203.7	17.6	0.295
S-2	30	60	71.9	1.695	2	40	3	203.7	17.6	0.295

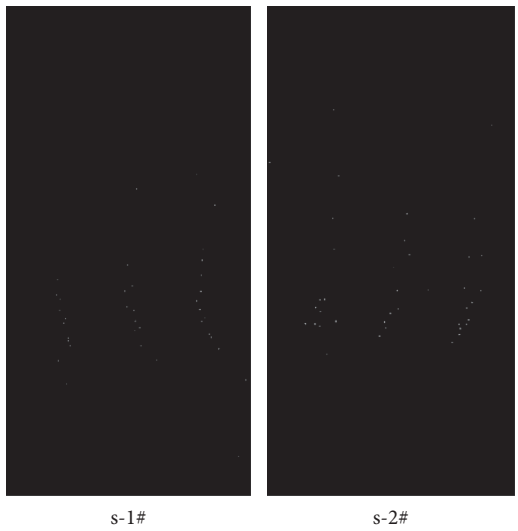

Figure 11: Picture of pit treatment on the witness plate after validation test.

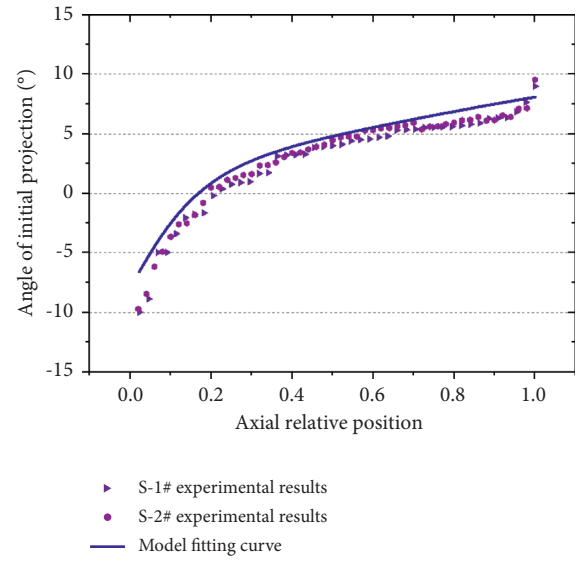

Figure 12: Test value of combat fragmentation dispersion distribution.

The calculated model data in this paper are compared with flying angle prediction results of Taylor and Flix et al. [7, 8] formulas, and the comparison results are shown in Figure 14. The prediction of the fragment's flying angle given by the Taylor formula was close to a straight line parallel to the X/L axis. When such a predicted result was compared with the experimental data, the correlation coefficient could not be estimated because the standard deviation of the predicted result was zero. By making a minor adjustment to the straight line, e.g., reducing the value of a selected point on the straight line by 10%, the correlation coefficient became approximately 0.3, indicating that the Taylor formula has little correlation with experimental data. As to the flying angle prediction model developed by Flix, although its predicted trend of the flying angle distribution was correct,

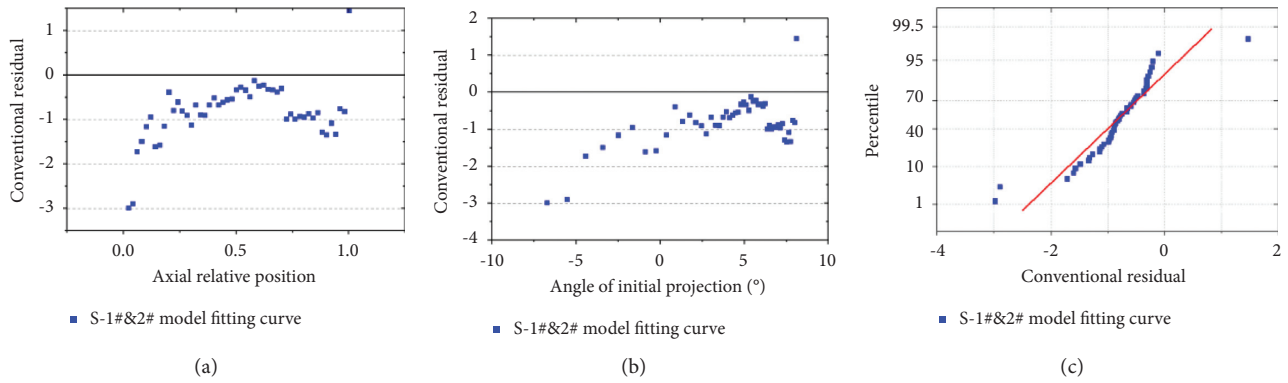

Figure 13: Error analysis for verifying the model. (a) Axial relative position error. (b) Dispersion distribution error. (c) Percentile error.

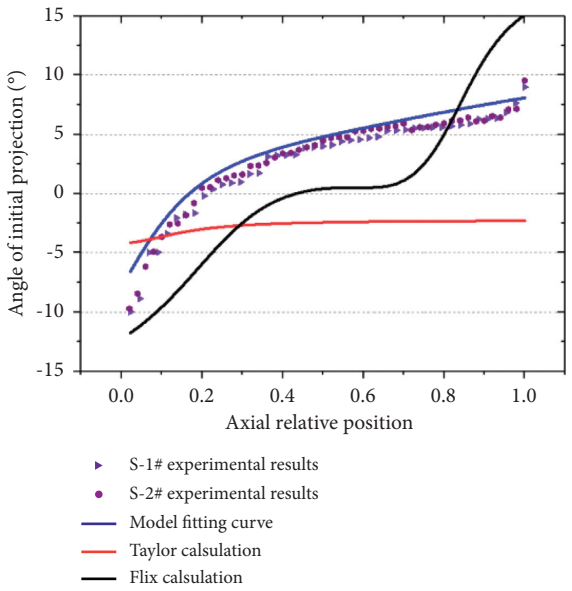

Figure 14: Comparison of empirical model.

its accuracy was poor compared with the actual data, especially at the detonation and nondetonation ends where the correlation coefficient was only approximately 0.64. Therefore, on the one hand, compared with the previous models, the proposed model in this study can accurately predict the flying angle distribution. On the other hand, the model still needs to be further improved for better accuracy. For example, for the fragment dispersion distribution at the remaining 3% axial positions near the tail of the nondetonation end, distribution errors need to be reduced and subject to future research.

6. Results and Discussion

In this study, the charge diameter and the ratio of charge mass to shell mass were varied to build different test samples to obtain the test data of a warhead fragment's initial velocity and flying angle under different conditions. The impact of the sparse waves on fragment dispersion was analyzed. A calculation model was proposed to predict fragment dispersion distribution under the effects of the axial sparse waves and the relative axial shell position under one-end detonation for cylindrical warheads. The model was completed by experimental data fitting. The research results show the following findings:

(1) Different warheads of the cylindrical charge with different aspect ratios were affected by the sparse waves from the two ends of the shell, showing similar nonlinear distributions. The middle fragments scattered steadily, and the fragments at the two ends scattered with larger deviations in the flying angle. The decrease or increase trend in the flying angle on both sides was related to the end effect of the sparse waves, especially in the dispersion distributions at the detonation and nondetonation ends. The impact of the sparse waves on the detonation end is greater than that on the nondetonation end. The flying angle presented a nonlinear distribution with two ends rising rapidly and the middle part increasing steadily.

(2) The proposed model was completed using curve fitting with experimental data based on the hyperbolic sine (sinhx) function curve. The model can accurately predict the fragment distribution under the impact of the sparse waves, especially the detonation and nondetonation ends. With the parameters of x/d and $(L - x)/d$, the model can predict the fragment dispersion distribution at each axial position of the warhead. The residual differences between the relative axial positions and the fitted Y values were between −1 and 1.5, and the conventional residual in the percentile was less than 0.3. The relative error in 97% of the data at all axial positions was within 3%. This means that the proposed model is more accurate than the previous models.

(3) A separate set of validation tests was designed to confirm the model's accuracy. The validation results showed that the relative errors in 97% of the data along the axial direction of the warhead were less than 6%, indicating good accuracy for different cylindrical warheads. The model is essential for the risk assessment of improvised explosive devices.

(4) Compared with the flying angle prediction results given by the Taylor and the Flix formulas, the

proposed model offers better accuracy, which is reflected by higher correlation coefficients than the test data, especially at the detonation and nondetonation ends. This fact points out the significance of addressing the impact of the end sparse waves on fragment dispersion unevenness.

However, this study still has some limitations, mainly because the model includes an empirical part that requires experimental data support. Therefore, more theoretical and test data analysis is needed in future improvement. In addition, the fragment dispersion distribution of the remaining 3% axial positions near the tail at the nondetonation end requires improvement to reduce errors. This study can guide the investigation of the fragment dispersion distribution of warheads of a noncylindrical shape and asymmetric charge.

Data Availability

The data used to support the findings of this study are available from the corresponding author upon request.

Conflicts of Interest

The authors declare that there are no conflicts of interest regarding the publication of this study.

Acknowledgments

The authors thank Dr. Dou Hong and Dr. Da-Cheng Gao, from the School of Mechanical Engineering, Nanjing University of Science and Technology for their suggestions on the revision of this paper, drawing charts, and paper formats. The work presented in this paper was supported by the National Program for Top Young Talents and Foundation Enhancement Program.

References

[1] S. Waggener, "Relative performance of anti-air missile warheads," in *Proceedings of the 19th International Symposium of Ballistics*, pp. 623–630, Interlaken, Switzerland, May, 2001.

[2] R. M. Lloyd, *Conventional Warhead Systems Physics and Engineering Design*, Vol. 179, American Institute of Aeronautics and Astronautics, , Reston, VA, USA, 1998.

[3] R. W. Gurney, *The initial velocities of fragments from bombs, shell and grenades*, Army Ballistic Research Laboratory, Aberdeen Proving Ground, MD, USA, 1943.

[4] G.-y. Huang, W. Li, and S.-s. Feng, "Axial distribution of fragment velocities from cylindrical casing under explosive loading," *International Journal of Impact Engineering*, vol. 76, pp. 20–27, 2015.

[5] T. Zulkoski, *Development Of Optimum Theoretical Warhead Design Criteria*Naval Weapons Center, China Lake, CA, USA, 1976.

[6] G. Randers Pehrson, "An improved equation for calculating fragment projection angle," in *Proceedings of the 2nd International Symposium on Ballistics*, pp. 223–226, Datona Beach, FL, USA, January, 1976.

[7] G. I. Taylor, "Analysis of the explosion of a long cylindrical bomb detonated at one end, Mechanics of Fluids," in *The Scientific Papers of Sir Geoffrey Ingram Taylor*, vol. 3, pp. 277–286, Cambridge University Press, Cambridge, UK, 1941.

[8] D. Felix, I. Colwill, and P. Harris, "Real-time calculation of the initial angle of projection for fragments in cylindrical warheads," *The Journal of Defense Modeling & Simulation*, Article ID 154851292098267, 2021.

[9] D. E. Carlucci and S. S. Jacobson, *Ballistics: Theory and Design of Guns and Ammunition*, CRC Press, Boca Raton, FL, USA, 2017.

[10] M. N. Deshpande, "91.04 the Pell sequence and Pythagorean triples," *The Mathematical Gazette*, vol. 91, no. 520, pp. 75-76, 2007.

[11] W. P. Walters and J. A. Zukas, *Fundamental of Shaped Charges*, Wiley, New York, NY, USA, 1989.

[12] P. C. Chou, E. Hirsch, and R. D. Ciccarelli, *An Unsteady Taylor Angle Formula For Liner Collapse,*Defense Technical Information Center, Fort Belvoir, Virginia, 1981.

[13] P. C. Chou, J. Carleone, W. J. Flis, R. D. Ciccarelli, and E. Hirsch, "Improved formulas for velocity, acceleration, and projection angle of explosively driven liners," *Propellants, Explosives, Pyrotechnics*, vol. 8, no. 6, pp. 175–183, 1983.

[14] C. Knock and N. Davies, "Blast waves from cylindrical charges," *Shock Waves*, vol. 23, no. 4, pp. 337–343, 2013.

[15] J. E. Kennedy, "The Gurney model of explosive output for driving metal," in *Explosive Effects and Applications*, J. A. Zukas and W. P. Walters, Eds., Springer, New York, NY, USA, pp. 221–257, 1998.

[16] G. Tanapornraweekit and W. Kulsirikasem, "Effects of material properties of warhead casing on natural fragmentation performance of high explosive (HE) warhead," *World Academy of Science, Engineering and Technology*, vol. 59, no. 11, pp. 1275–1280, 2011.

[17] W. J. Flis, "Analytical models of the projection angle of explosively accelerated liners," in *Proceedings of the 15th International Symposium on Ballistics*, pp. 243–251, Jerusalem, Israel, 1995.

[18] M. Wang, F. Lu, X. Li, and L. Cao, "A formula for calculating the velocities of fragments from velocity enhanced warhead," *Propellants, Explosives, Pyrotechnics*, vol. 38, no. 2, pp. 232–237, 2012.

[19] L. Qian, T. Liu, S. Zhang, and Y. Yang, "Fragment shot-line model for air-defence warhead," *Propellants, Explosives, Pyrotechnics*, vol. 25, no. 2, pp. 92–98, 2000.